JOURNAL OF AIRCRAFT
Vol. 30, No. 5, Sept.–Oct. 1993

Induced Drag of a Crescent Wing Planform

F. Lam* and D. J. Maull†
University of Cambridge, Cambridge CB2 1PZ, United Kingdom

Comparative study, both computational and experimental, has been carried out on the possible drag reduction at low speeds of two wings of same aspect ratio 6, but different wing planforms; one is crescent and the other is elliptic. Computational results, using two inviscid panel programs, indicate that the crescent wing planform is capable of reducing the drag, interpreted from the integrated surface pressure distributions. The benefit has been attributed to a high suction pressure loading in the tip region in the case of the crescent wing. However, such a potential in drag reduction cannot be verified experimentally at the Reynolds number based on the mean chord 0.25×10^6. There has been no expected gain in the effective aspect ratio associated with the crescent wing, based on the results of balance tests. Detailed wake surveys at a downstream distance behind these wings reveal substantial differences in the wake structures at an approximate lift coefficient of 0.35, but the vorticity in the wake vortex cores shows similar magnitudes. One explanation for the misleading computational findings is that there exists a residue drag at no-load condition, possibly arising from the errors in the discretization of the highly curved tip shape. This residue drag tends to contaminate the calculation at lifting conditions.

Nomenclature

a = $\partial C_L/\partial\alpha$ of wing
a_0 = $\partial C_L/\partial\alpha$ of two-dimensional section
AR = aspect ratio of wing, $2b/\bar{c} = 4b^2/S$
b = wing semispan
c = section chord of wing
$\bar{c}$ = mean aerodynamic chord of wing
c_l = sectional lift coefficient, $l/q_\infty c$
C_D = overall drag coefficient, $D/q_\infty S$
C_{DI}, C_{DII} = drag components defined by Eqs. (5) and (6)
C_{DP}, C_{DV} = coefficients of profile and vortex drag, respectively
C_L = overall lift coefficient of wing, $L/q_\infty S$
Cp = static pressure coefficient, $(p - p_\infty)/q_\infty$
Cp^* = total head coefficient, $(H_\infty - H)/q_\infty$
C_S = side force coefficient, $S_F/q_\infty S$
D = drag
e_i = $\partial C_D/\partial C_L^2$
H = total pressure or head
k_i = induced drag factor defined in Eq. (1)
L = lift
N_y, N_z = total grid numbers in y and z direction, respectively
p = static pressure
q = dynamic head $\frac{1}{2}\rho U^2$
Re = Reynolds number
S = planform area of wing (projected area on z = 0 plane)
S_F = side force—positive away the root of wing
U = velocity in x direction
U_e = effective velocity defined in Ref. 17
$U^\star$ = velocity defined in the Betz's hypothetical flow
u, v, w = perturbation velocity components in x, y, z directions
x, y, z = rectangular Cartesian coordinates: x, freestream direction; y, starboard; and z, upward
α = angle of incidence
ζ = z/b
η = y/b
ξ = vorticity component defined by $\partial w/\partial y - \partial v/\partial z$
ρ = air density
Ψ = stream function of crossflow

Subscripts
rt = root of wing
t = downstream traverse plane
∞ = freestream undisturbed condition

Superscripts
w = wake region
$-$ = denotes nondimensional quantities

Introduction

ACCORDING to the linearized theory of finite-aspect ratio wings, the total drag can be conveniently separated into two components for a monowing[1]:

$$C_D = C_{D_0} + C_{D_i} = C_{D_0} + (k_i C_L^2/\pi AR) \tag{1}$$

The first component is called the profile drag which is associated with the boundary layers on the surfaces of a wing. The second is the induced drag arising from the creation of a trailing vortex sheet as a result of generating lift. The value of k_i is a function of spanwise loading only, and achieves its theoretical minimum of unity with an elliptic loading.[2] The downwash in this case is constant across the span (and the chord as well). The effect of aspect ratio may be generalized by the function f, below, to relate to the lift slope of the corresponding two-dimensional airfoil section

$$\frac{\partial C_L}{\partial\alpha} = \frac{a_0}{1 + f(1/AR)} \tag{2}$$

In the present study we are concerned with only a particular type of planform. In a systematic investigation of wing planform of soaring birds, Zimmer[3] deals with the induced drag characteristics of natural planforms in the light of classical wing theory strengthened by the vortex lattice modeling technique. Although no physical evidence is presented to support the claim, an aft-swept triangular tip, e.g., a planform similar to that of an albatross, is identified to have the advantage of 3–4% lower induced drag than a planar elliptic planform.

Received June 14, 1991; revision received May 20, 1992; accepted for publication May 27, 1992.

*Research Associate, Department of Engineering, Trumpington Street.
†Reader in Engineering Fluid Mechanics, Department of Engineering, Trumpington Street.

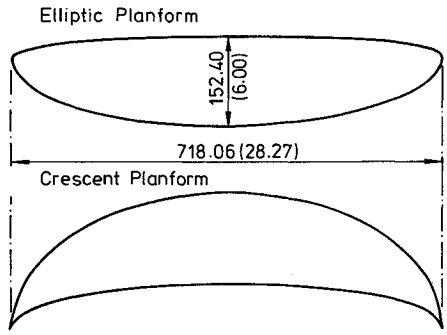

Fig. 1 Two wing planforms, all dimensions in mm (in.).

Initiated by this study, van Dam[4] further analyzes the induced drag characteristics of several aft-swept triangular tips on the outboard portion of a nontwisted unswept wing by an inviscid surface panel method.[5] The beneficial effects are in general agreement with the findings of Zimmer.[3] Wind-tunnel experiments appear to confirm the advantage.[6] Although there is no obvious gain in the effective aspect ratio (inferred from the experimental $\partial C_L/\partial\alpha$), the nonlinearity of the tip at incidence and its influence on the wake deformation and pressure distribution are referred to as the sources of the benefit. Similarly, van Dam considers the curved wing planforms defined by the following expression:

$$c(\eta) = c_{r_t}\sqrt{1 - \eta^2} \tag{3}$$

This series of planforms looks like the lunate tails of large aquatic animals or the wing of a swift. In particular, he finds that a planform formed by two ellipses of $c_{r_t} = 1.5$ and $c_{r_t} = 1.0$ has a 8% lower value in k_i than the theoretical minimum value of unity of an elliptic planform wing of the same aspect ratio 7. Similar results are also reported[7] based on the outcome of a different panel program.[8] Experimental investigations by balance measurements performed by van Dam et al.[9] tend to confirm the claim, but only with a 1–2% gain in k_i, with no apparent increase in the effective aspect ratio (again judged from the lift against incidence curves). Above all, their value of k_i is not below the theoretical minimum. However, an aft-swept and tapered tip on the end of unswept basic wings (aspect ratios 8 and 11, respectively) is found to have penalties in the induced drag under the experimental conditions[10] compared with an elliptic tip. Furthermore, a recent analysis[11] pointed out a source of error in the analysis.[4] The convergence of the induced drag resulting from the integration of the chordwise pressure distribution through the wing thickness is a slow function of the number of spanwise panels for a given chordwise panel distribution for a given wing shape. The recalculated k_i is confirmed not to be lower than the theoretical minimum.

In this article an attempt is made to find where the benefit comes from, if there is any. Using two panel methods, a computational study is performed. A comparison of the predictions is made with balance measurements interpreted in terms of the classical wing theory. Considerable efforts are spent on detailed wake surveys behind wings. Two planforms were selected for comparative study (see Fig. 1). Both wings have the same airfoil section, span, and chord distribution (i.e., the same aspect ratio 6). The first planform is "elliptic" and the other with a highly aft-swept tip is "crescent." The airfoil section is a symmetrical NACA 0009. The wings are made of aluminum alloy and were machined to a high degree of surface finish. Transition is fixed at 5 and 10% local chord positions on both surfaces using roughness bands[12] of about 1-mm wide.

Computations

Two panel methods, VSAERO[5] and SPARV,[8] have been used in the present study for the aerodynamic analysis of the wing planforms. Some important features, common to these methods, are briefly discussed here.

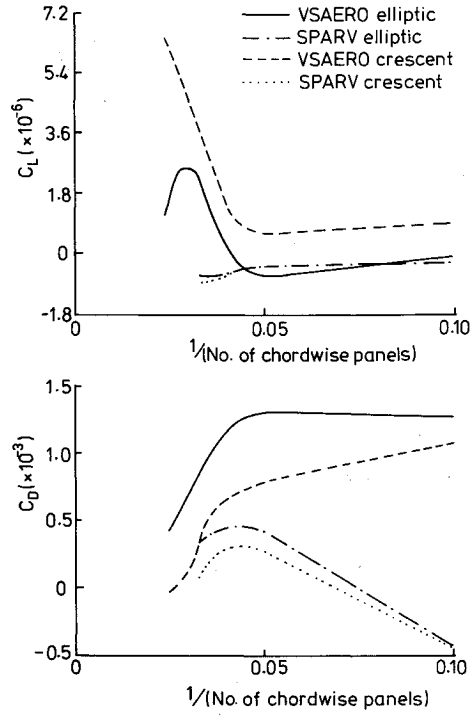

Fig. 2 Residue C_L and C_D in panel methods.

Experience has shown that there is a residue coefficient at each wing geometry with each paneling case at $C_L = 0$. This is assumed to exist at higher C_L, and therefore, a true value is calculated as

$$C_L = C_{L(\text{calculated})} - C_{L(\text{residue})} \tag{4}$$

The same applies to C_D and C_S.

It is expected that the wake relaxation is essential in determining the induced drag. As the number of the spanwise wake elements is limited by the available number of panels on the wing, an effort has successfully been made to modify one of the codes (VSAERO) so that it has the capacity of handling up to 90 wake panels per wake line. For a given streamwise length of wake line, even denser paneling is made possible without excessive increase in computational time and storage.

In order to confirm the finding by other researchers, computations using inviscid panel methods were carried out with different input panel parameters for the given wing shapes. Since the total number of panels for a given wing geometry depends largely on the resources and memory available, it was found that a discretization with 800 surface panels with three wake relaxation cycles was the maximum computational limit on the IBM 3084 MVS mainframe system. To ensure a sufficient number of panels used on a chordwise location to predict reasonable leading and trailing-edge flows, the effects of chordwise panel number on residue C_L and C_D were first examined (Fig. 2) at a fixed spanwise station 10.

The residue values of lift and drag are the integrated results from a panel program for a particular paneling under no lift condition in the absence of a wake. The airfoil section is symmetric so the residue values should be computationally zero. The residue C_L is indeed negligible over the range of chordwise paneling, but the residue C_D is significant over the test range. In Table 1, the percentage of residue C_D at $C_L = 0$ out of the C_D in a lifting case is shown, using 30 panels on each upper and lower surface and 10 spanwise stations. Use of SPARV to model a sharp-pointed wing tip was hindered by a numerical instability so that in the present study the wing tips were cropped by a small length of 5% of the wing root

chord. This may partly explain why the residue C_D was lower using SPARV. Therefore, it is important to take the residue C_D into account. An analysis of the results in Ref. 4 showed a residue C_D of about 5% on a wing of the elliptic planform using 1000 surface panels by VSAERO. It must be kept in mind that uncertainty still arises on the value of the drag, even with removal of the residue drag.

In Table 2 the results of computations on the two wings by the two panel methods are listed. The calculations were performed with 600 surface panels with a roughly constant lift coefficient of 0.35. Additional iterations using VSAERO were computed and no significant variations in the coefficients were found. The calculated k_i based on aspect ratio 6 are worked out in Table 3. Reference is made with the minimum induced drag factor unity of classical wing theory. The figures in brackets show the percentage of the reduction. The figures behind the elliptic wing are referred to the theoretical minimum and those of crescent are deviated from the values of the elliptic wing. Both panel methods predict the reduction in the induced drag for the crescent planform, although there is a large discrepancy. The spanwise loading is presented in Fig. 3 where an increased loading on the tip for crescent wing is shown. An ellipse is superimposed on the plot, and the elliptic wing shows close agreement with the optimum loading.

An attempt was made to pinpoint the source of the potential drag reduction by the crescent planform. The pressure distributions of VSAERO were plotted in Figs. 4 and 5. The Kutta condition is not exactly satisfied at the last one or two spanwise stations near the tip regions in both wing cases. This is most likely caused by the numerical error incurred by the denser paneling in these regions. As the induced drag is a

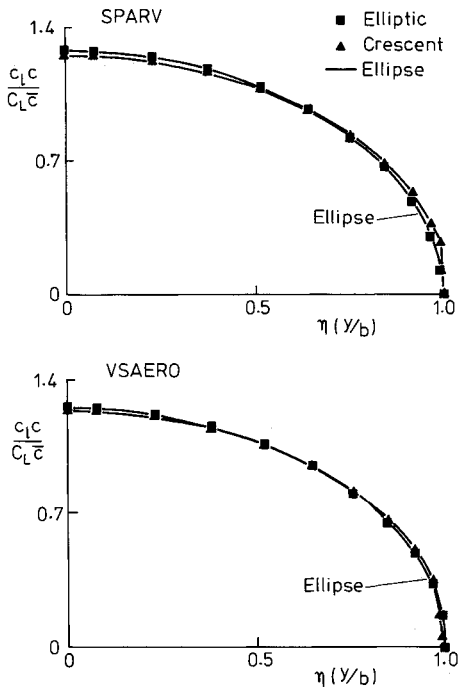

Fig. 3 Spanwise loading by SPARV and VSAERO.

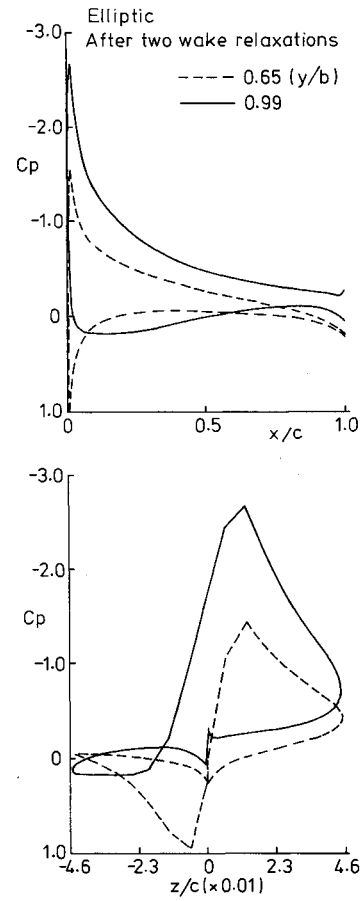

Fig. 4 Pressure distributions on elliptic wing by VSAERO.

Table 1 Panel method residue drag as a percentage of total drag at $C_L \approx 0.35$

	Elliptic wing		Crescent wing	
Wakes	VSAERO	SPARV	VSAERO	SPARV
0	12.9	4.8	6.2	1.8
1	11.9	4.7	6.0	1.8
2	11.9	4.7	6.1	1.8

Table 2 Results of calculation by panel methods

	Elliptic wing				Crescent wing			
	VSAERO		SPARV		VSAERO		SPARV	
Wakes	C_L	$C_{D_i} \times 10^{-3}$	C_L	$C_{D_i} \times 10^{-3}$	C_L	$C_{D_i} \times 10^{-3}$	C_L	$C_{D_i} \times 10^{-3}$
0	0.355	6.5	0.362	7.2	0.345	5.6	0.353	5.5
1	0.358	7.0	0.362	7.4	0.346	5.7	0.353	5.6
2	0.359	7.1	0.361	7.4	0.346	5.7	0.353	5.6

Table 3 Reduction of the induced drag factor

	Elliptic wing		Crescent wing	
Wakes	VSAERO	SPARV	VSAERO	SPARV
0	0.9702(−2.98)	1.0404(4.04)	0.8858(−8.70)	0.8361(−19.64)
1	1.0352(3.52)	1.0723(7.23)	0.9025(−12.82)	0.8456(−21.14)
2	1.0376(3.76)	1.0737(7.37)	0.8989(−13.37)	0.8465(−21.16)

result of pressure integration through the thickness of the wing, the negative drag or suction near the curved tip on the crescent wing is responsible for the overall drag reduction shown by the total drag. A similar situation was found for another crescent wing by means of SPARV.[7] One of the reasons for the existence of the favorable pressure could be "a sidewise suction force" on the leading-edge regions of the highly curved tip. The downwash on the upper surface is drawn in Fig. 6. Compared to that predicted by the lifting-line theory[13] for the given lift and the aspect ratio, the chordwise downwash distribution shows that it varies over chord, especially in the leading-edge region. Both wings indicate a nearly constant spanwise downwash, except perhaps in the tip area, as shown from the classical theory for finite-aspect ratio wings with elliptic loading.

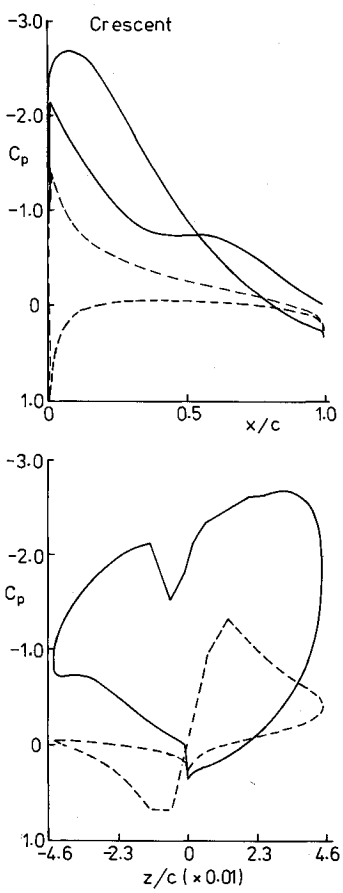

Fig. 5 Pressure distributions on crescent wing by VSAERO.

Experimental Tests

The tunnel used for the experiments is a closed-circuit one in the Aerodynamics Laboratory of the Engineering Department at the University of Cambridge. The working section is 1.68-m wide and 1.22-m high, and it has an octagonal cross section with corner fillets. The longitudinal dimension in the axis direction is about 3.5-m and the cross section is slightly divergently tapered downstream to compensate for the growth in the displacement thickness of the wall boundary layers in order to maintain a constant pressure throughout the entire working section. The slots at the rear of the working section tend to equalize the static pressure in the working section and the atmospheric pressure outside the tunnel. The freestream turbulence level, namely a root mean square (rms) of u component fluctuation compared with the mean velocity, was found to be 0.22% at a tunnel mean speed of 30 m/s. This is considered to be satisfactory for the present application.

A three-degree-of-freedom traverse gear was designed and installed at the external rear working section of the tunnel with some wall slots to allow for the movement of a probe. The probe used to explore the highly three-dimensional flowfield is a one-tube fixed-direction yaw-meter originated by Chu[14] with some improvements.[15] The advantages of using a one-tube yaw-meter together with the pull/push accessory are 1) we have a well-defined, single position with minimal measuring volume, typically ~1 mm^3, with the information of the local total head; and 2) the fast action of the adjustable switch-on time solenoid aims to shorten the time consumed during probe hardware manipulation, while at the same time allow sufficient time to take the required number of samples. For details of these experimental apparatus and conditions, the reader is referred to the references just cited. Wake surveys using the probe and the traverse mechanism described earlier were carried out at a fixed downstream distance of roughly three root chord lengths behind the roots of the wings. Nonuniform survey meshes were used in order to cut down the tunnel running time with typical 4 mm in the core and trailing-edge wake regions, and 8 mm in other areas. The angle of incidence was 5.17 deg and was the same for both wings. Balance results indicated a lift coefficient of about 0.35 at this incidence. It was believed that the wing-tip flow is not an isolated event and is related to the overall loading of complete wing which is determined by the trailing edge.

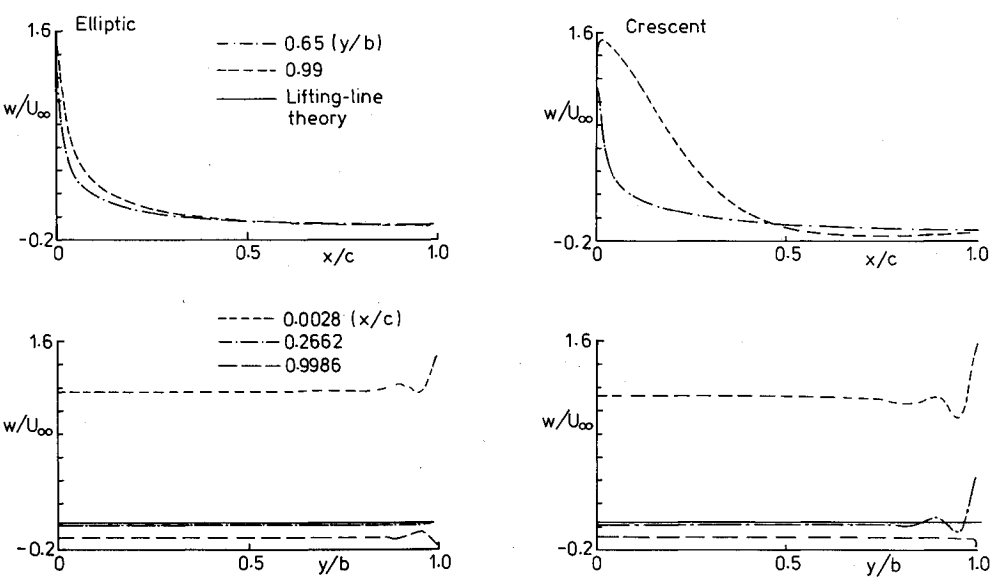

Fig. 6 Downwash distributions calculated by VSAERO.

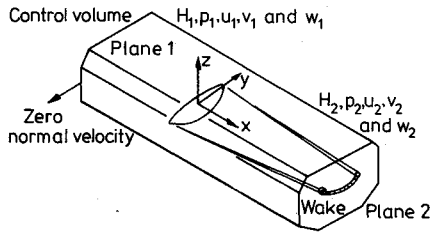

Fig. 7 Control volume analysis of lifting wake.

Theory for Wake Survey

The application of momentum principle to a control volume (Fig. 7) between two upstream and downstream vertical planes (denoted by 1 and 2) for the evaluation of the aerodynamic forces (expressed in terms of coefficients) in any traverse plane, cut through the wake in a steady, incompressible, and homogeneous fluid, leads to[15-17]

$$C_{D_I} = \sum_{k=1}^{N_z} \sum_{j=1}^{N_y} [Cp^* + (\bar{U}_t^* - \bar{U}_t)(\bar{U}_t^* + \bar{U}_t - 2\bar{U}_e)]_{jk}^w \quad (5)$$

$$C_{D_{II}} = \sum_{k=1}^{N_z} \sum_{j=1}^{N_y} [\bar{\Psi}\bar{\xi}]_{jk}^w \quad (6)$$

$$C_L = 2 \sum_{k=1}^{N_z} \sum_{j=1}^{N_y} [\bar{U}_e \bar{\xi} y + (\bar{U}_t^* - \bar{U}_t)\bar{w}_t]_{jk}^w \quad (7)$$

$$C_S = 2 \sum_{k=1}^{N_z} \sum_{j=1}^{N_y} [\bar{U}_e \bar{\xi} z + (\bar{U}_t^* - \bar{U}_t)\bar{v}_t]_{jk}^w \quad (8)$$

The advantage of separating the total drag into two constitutes is apparent. The first part, C_{D_I}, is associated with the total pressure deficit in the wake behind the wing, together with a small term for the tunnel correction. A substantial amount of the component comes from the viscous shearing flow in the boundary layers. The second component, $C_{D_{II}}$, is solely connected with the large-scale, predominantly inviscid rotational motion of fluid, excluding the viscous core of rolled-up vortex, where large total head losses are frequently realized. The importance of the vorticity distribution in the wake is further stressed in Ref. 18.

If the existence of a rolled-up vortex core is attributed to the initial rotational motion, manifested as the vortex flow in the immediate neighborhood of the trailing edge, there should be an additional part, namely δC_{D_c} in $C_{D_{II}}$ due to the total pressure losses of the vortex core. Thus

$$C_{D_P} = C_{D_I} - \delta C_{D_c}, \qquad C_{D_V} = C_{D_{II}} + \delta C_{D_c} \quad (9)$$

With the continuous rolling-up of the trailing vortex sheet, a variation of δC_{D_c} with downstream distance is expected, as a test case behind a bluff body shows.[19] However, if the survey planes are limited to less than a length of three or four mean chords behind a wing, the definitions of C_{D_I} and $C_{D_{II}}$ can be unique.[20] Naturally, wake surveys for the comparative study of wing configurations with similar longitudinal dimensions can be carried out at fixed downstream transverse locations. The ultimate definitions of the drag components are best settled in the light of the experimental results.

Complete Wakes

The contours of the total head deficit shown in Figs. 8 and 9 indicate that there is a higher total head loss in the core of the crescent wing wake. This corresponds to a more tightly rolled up vortex core. A region of nonuniform total pressure distribution exists in the wake of the crescent wing just outside the core area. The trailing edge wakes are similar in the two cases with a thicker wake on the upper part, probably as a

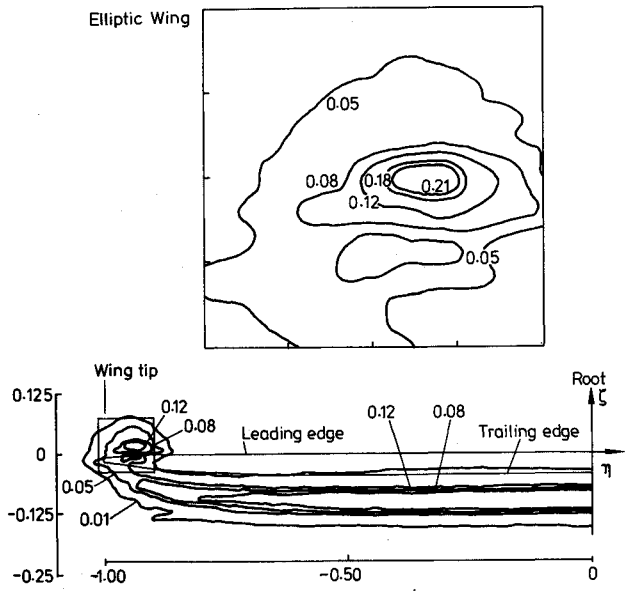

Fig. 8 Contour of Cp^* for elliptic wing on "port" side.

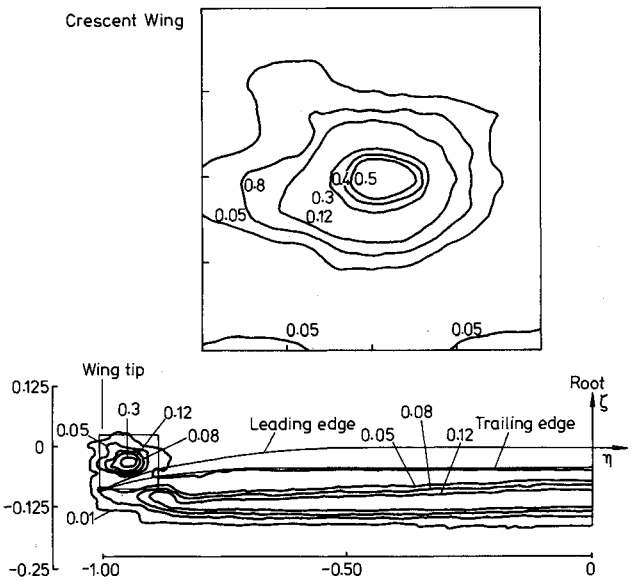

Fig. 9 Contour of Cp^* for crescent wing.

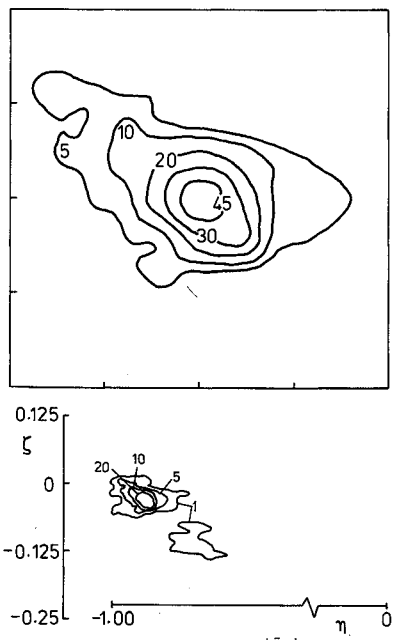

Fig. 10 Vorticity distribution $|\bar{\xi}b|$ (elliptic wing).

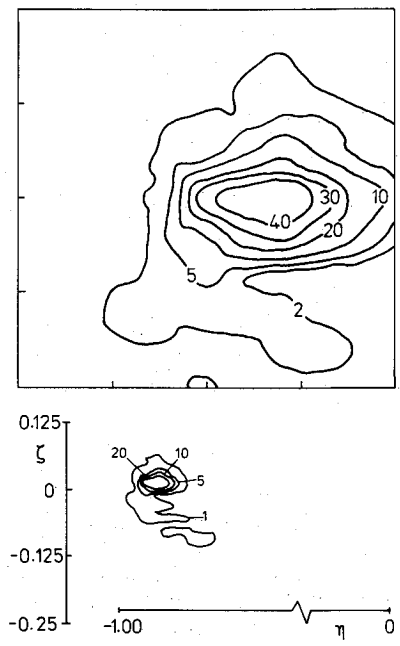

Fig. 11 Vorticity distribution $|\xi b|$ (crescent wing).

result of thicker boundary layers on the wing upper surfaces. The contours of the vorticity distribution are shown in Figs. 10 and 11. The vortex sheets seem to have completed their rolling-up process in both wing cases as shown by the concentration of strong vorticity around the core regions, though there is no great deal of difference in the mean distribution of the vorticity. The insets in these plots show the core region of the vortices.

Core Regions

As indicated by the total head loss, a considerable amount of the information is contained within the core regions of the rolled-up wakes. The maximum total pressure loss measured in the core of the crescent wing is nearly double that of the elliptic wing. This is indicative of the amount of energy contained in such small cross sections. The center of the core of the elliptic wing vortex is found to shift inboard and downward more than that of the crescent wing. This is probably because the survey plane is relatively further downstream behind the tip of the elliptic wing so that the trailing vortex rolled up to a larger extent behind the elliptic wing. The vorticity values (Figs. 10 and 11) indicate the elliptic wing has a wake vorticity being spread out over a larger area with slightly lower magnitudes. This means the kinetic energy contained in the wake is lower than that in the wake of the crescent wing. The core of the elliptic wing vortex tends to be elliptic with the major axis being parallel with the y-axis. While the core of the crescent wing vortex appears to have the vorticity axis inclined at roughly 45 deg to the horizontal axis.

The crossflow velocity vectors in Fig. 12 show the increased resultant velocities in the case of the crescent wing in the vicinity of the core regions; the stronger velocity components are also illustrated in Figs. 13 and 14. It is interesting to note that the axial velocities are roughly equal to that of the freestream value for the elliptic wing, while those of the crescent wing show lower values. In particular, the axial velocity near the core area in the case of the crescent wing shows the tendency of deceleration, i.e., negative perturbation. (Note that, the probe as described in Ref. 15 will not measure any negative variation in velocity.) The portion of fluid about to enter the core region, those with lower values of η and ζ, shows the decelerated axial velocity in the case of the crescent wing, compared to the elliptic wing.

The relationship between the various findings just described can be established in the light of wake survey theory and the requirement of dynamic equilibrium and continuity in rotating

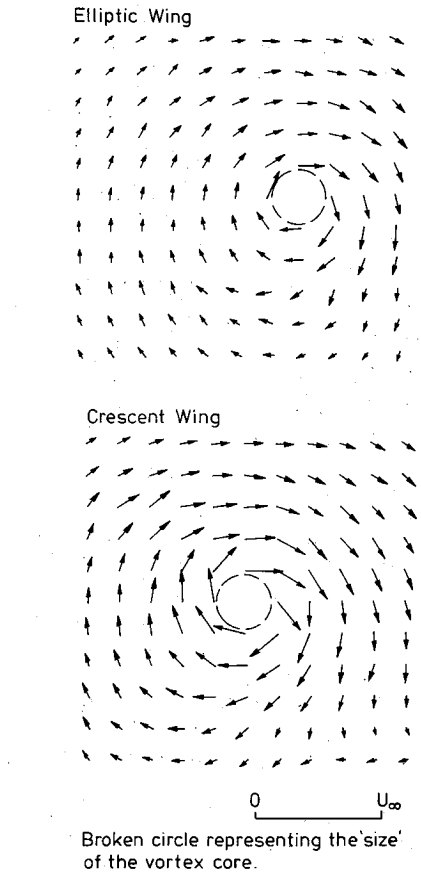

Fig. 12 Crossflow velocity vectors in the core regions.

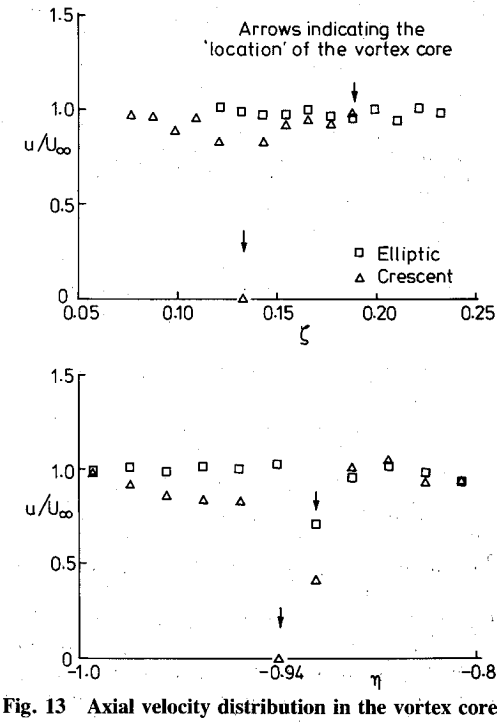

Fig. 13 Axial velocity distribution in the vortex cores.

fluid.[21] The variation of the total head over a plane normal to the freestream direction in a steady, homentropic, and effectively inviscid fluid is proportional to the axial vorticity with the proportional constant being one of the crossflow velocity components.[22] Comparison of the velocity distributions of the two wing cases shows the higher velocity components in the crescent wing on the same vorticity lines. On the other hand, the vorticity of the crescent wing is stronger at the points of the same velocity than that of the elliptic wing.

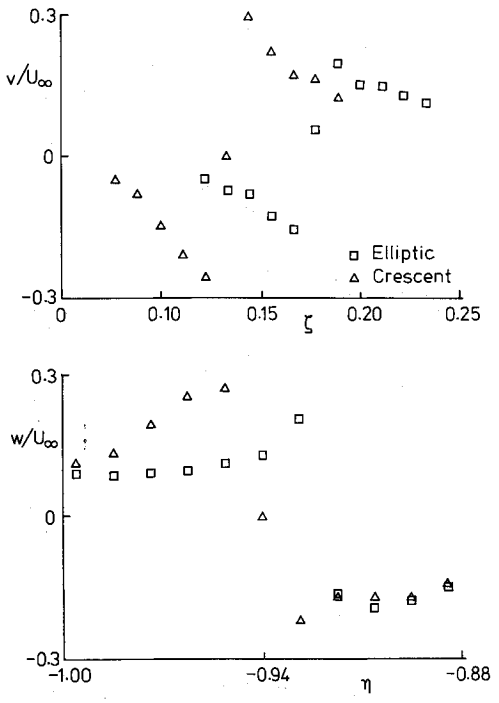

Fig. 14 Crossflow velocity distribution.

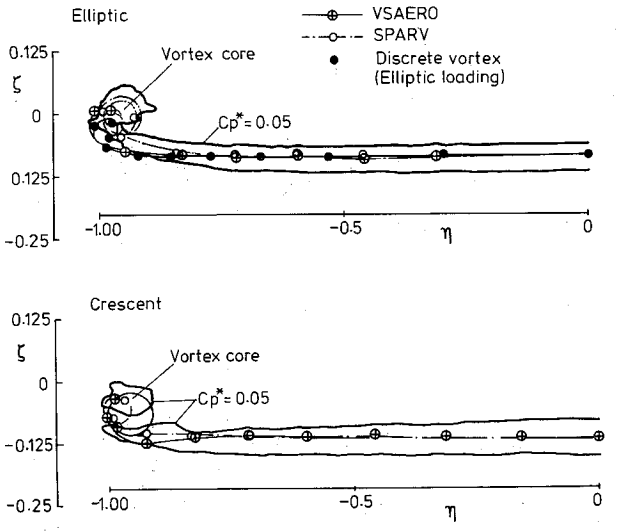

Fig. 15 Comparison between computations and experiments.

These two related effects lead to the higher total head loss. The enhanced swirling motion of the surrounding fluid around the core of the crescent wing wake gives rise to the important consequence of the tightening of the trailing vortex sheet. One can postulate the following picture of the flowfield existing around the rear-pointed crescent wing tip. The pressure on the suction side around the tip region is higher than the inboard region where higher suction is expected to produce higher loading. The external pressure outside the wake creates an axial adverse pressure gradient which will persist continuously along the core region and decelerate the axial motion of the fluid elements which enter the core under the influence of rolling-up. The higher vorticity values, and therefore, the second component of the drag is a direct consequence of the increased magnitudes of the crossflow velocities.

Comparisons with Computations

The comparison between the experiments and computations (see Fig. 15) indicates that the wake relaxation used in the panel methods predicts the position of roll-up reasonably well, although the inviscid methods cannot be regarded as a reliable representation of the induced crossflow velocity field in the traverse plane, especially in the rolled-up core regions. The result using a discrete vortex method,[23] assuming an elliptic loading also shows good agreement with the experiment.

Analysis of Aerodynamic Forces

Balance experiments were carried out at a Re_c of 0.25×10^6. Lift, drag, and pitching moment were measured over a range of incidences up to stalling. All the results are subject to the conventional tunnel corrections and necessary repeatability tests.[15] Figure 16a shows the lift as a function of incidence. It is found that there is no appreciable difference in the slope in the two wing cases (see Table 4). This means no useful gain in the effective aspect ratio as given in the classical wing theory. The crescent wing exhibits a higher stalling angle of incidence which is in agreement with that found elsewhere.[24] The theoretical curves indicate a reduced effective aspect ratio for the crescent wing planform by both panel programs. The discrepancy between the theoretical predictions and the experiments may be attributed to the viscous effects. The total drag as a function of lift is shown in Fig. 16b. The profile drag (the experimental drag at zero lift) in each case is added to the results due to theory in order to make a better comparison. Although the profile drag of the crescent wing has a lower value, the total drag at lifting conditions (e.g., at $C_L = 0.35$) still shows no apparent reduction in drag.

In Table 4, the aerodynamic forces and their relevant components are critically reviewed in the light of both experimental and theoretical evidence. Computational results by means of the panel methods are based on the valuations to give a lift coefficient close to that obtained in the experiments. A fixed tare drag due to the wires and sting has been deducted from the measured drag. (This correction is between 20–60% of the measured value, depending on the incidence.)

Good agreement between the balance tests and the results of wake survey is obtained. Analysis of balance results according to the classical wing theory shows the induced drags of the crescent and elliptic wings are in fact equal, taking into account of the variation in lift and experimental errors.[15] There is no useful gain in the effective aspect ratio of the crescent wing. The wake survey indicates the induced drag is slightly higher for the crescent wing with higher lift based on the

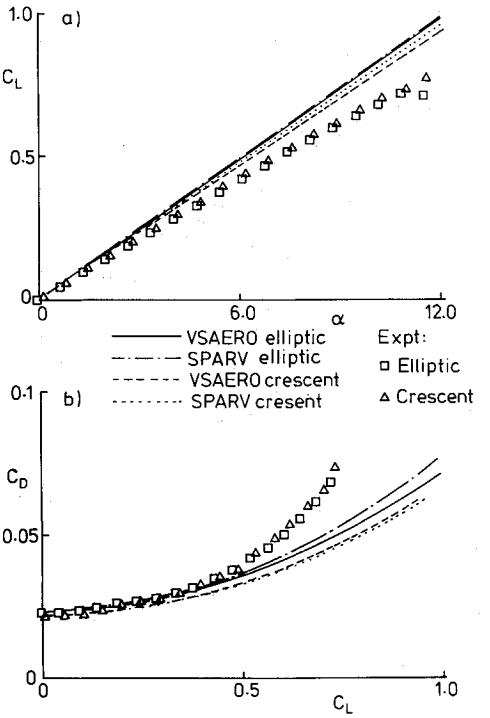

Fig. 16 Results of balance tests: a) lift as a function of incidence, and b) total drag as a function of lift.

Table 4 Analysis for aerodynamic forces of the crescent and elliptic wings

	Crescent wing				Elliptic wing				
	VSAERO	SPARV	Balance	Wake	VSAERO	SPARV	Balance	Wake	Lifting-line
C_L	0.346	0.351	0.361	0.348	0.359	0.361	0.362	0.342	0.360
C_{D_0}			0.0221				0.0231		
C_{D_I}				0.0239				0.0227	
C_{D_P}				0.0230				0.0224	
C_{D_i}	0.0057	0.0056	0.0093		0.0071	0.0074	0.0090		0.0069
$C_{D_{II}}$				0.0091				0.0088	
C_{D_V}				0.0100				0.0092	
C_D			0.0314	0.0330			0.0321	0.0315	
a	4.4579	4.5627	4.0046		4.7305	4.7038	4.0172		4.7124
e_i	0.0457	0.0443	0.0733		0.0484	0.0545	0.0731		0.0531
C_S	0.5457	0.5480		0.5361	0.5401	0.5500		0.5601	
k_i	0.8989	0.8465	1.3820	1.5602	1.0376	1.0737	1.3785	1.4802	1.0000

Table 5 Induced drag factors as a function of the number of data points

	Crescent wing					Elliptic Wing				
	10	9	8	7	6	10	9	8	7	6
e_i	0.0823	0.0781	0.0733	0.0659	0.0650	0.0801	0.0765	0.0731	0.0698	0.0650
k_i	1.5517	1.4727	1.3820	1.2420	1.2243	1.5089	1.4412	1.3785	1.3153	1.2247

theory for the wake survey. Both crossflow velocity distributions and total pressure results, particularly in the core regions, support the interpretations. By taking into account these facts, it is found that the induced drag characteristic is almost identical for both the elliptic and the crescent wing planforms in the present experimental conditions. The slightly heavily loaded tip on the crescent wing, as predicted by the inviscid panel methods, may be considered as the source for the more tightly rolled-up trailing vortex core. Strong perturbation in the axial velocity is also responsible for the existence of such concentrated vortex core. Both the nonplanarity and features of the trailing vortex sheet near the wing trailing edge might be fully investigated to explain the findings. The nonplanarity of the crescent wing, as viewed from downstream, tends to prevent the trailing vortex from shifting away from the tip regions. The location of the tip vortex core and the vorticity distribution are required to assess the effectiveness of a given aspect ratio, because the evaluations of lift and the induced drag from the wake survey depend also on the magnitude of the streamwise vorticity. The present study finds no physical evidence to support the benefit claimed by the results of panel methods, although it should be appreciated that panel methods using very large computers have shown,[11] very recently, that the benefits claimed from the earlier panel calculations are likely to be incorrect. Perhaps detailed surface pressure measurements will provide further crucial information on the findings from the panel methods.

The relatively high values of k_i in both wing cases were explained by the following arguments. The wing was lightly loaded with small dimensions and it was limited by scaling effect. The viscous effect was strong and dominant in low-lift conditions. The relative errors in the velocity measurements in the situation of wake survey were likely to be high and it was likely to overestimate the final integrated results. Next, the evaluations of k_i in the case of the balance tests were carried out over a large range of incidence. This tends to increase the final results, although it is not clear how many data points should be used. In Table 5, the effects of the number of data points used to calculate e_i can be realized.

The range of lift coefficients over which the calculations were carried out is roughly from 0.235 to 0.644 for elliptic wing and from 0.199 to 0.618 for crescent wing, respectively. The values of the lowest C_L in each wing case were fixed so that the number of points used in the estimation indicated the first few points in these ranges. The accuracy in the final values of k_i was estimated to be $\pm 3\%$ in both cases. However, these shortcomings are not expected to invalidate the conclusions of this comparative study.

Conclusions

Panel methods, for the discretization of a given wing geometry, are powerful in the initial development of a new wing design, especially in the evaluation of lift. The induced drag, computed by the surface integration of pressures associated with the inviscid velocity field over the wing, must be interpreted with care before any definite conclusion may be drawn. It is vital to examine the relative accuracy in the induced drag caused by the presence of the residue drag, which is one of the possible uncertainties arising from the approximation. The residue drag depends largely on the numerical procedures developed in a particular program formulation and on the convergence of the integrated aerodynamic results with surface paneling. Useful checks may be made by examination of the pressure distributions and by comparison with the classical wing theory (i.e., Trefftz plane analysis) based on spanwise loading distribution which is readily acceptable because of the reliable evaluations of the sectional lift.

The wake relaxation procedure in the panel methods needs to be improved by employing more sophisticated techniques in the prediction of the mean effect of rolling-up behind conventional wings, at least for relative short downstream distances. Agreement is poor in the cores because of strong viscous effects there and the singular behavior of the inviscid vortex elements.

Both balance measurements and the wake survey at the Reynolds number of 0.25×10^6 indicate that the untwisted crescent wing planform shows no obvious advantages over the elliptic wing in the induced drag in the present experimental conditions. The nonplanarity of the crescent tip at incidence causes increased tip loading as predicted by the panel methods, and appears to be responsible for the more tightened rolled-up vortex core and strong perturbation in axial velocity compared to that behind the elliptic wing. Since the structures of the wake are found very interesting, further work should concentrate on the detailed flowfield study at several downstream locations, in particular on the core areas of the trailing vortices.

Acknowledgments

F. Lam would like to thank the Croucher Foundation and its Trustees for providing a scholarship while this research work was being undertaken. Thanks also go to M. Gaster for discussions and advice throughout this research. Some of the equipment was bought from a grant from British Aerospace plc.

References

[1]Prandtl, L., "Application of Modern Hydrodynamics to Aeronautics," NACA Rept. 116, 1921.

[2]Munk, M. M., "The Minimum Induced Drag of Aerofoils." NACA Rept. 121, 1921.

[3]Zimmer, H., "The Aerodynamic Optimisation of Wings at Subsonic Speeds and the Influence of Wingtip Design," Translation of Dr.-Ing. Dissertation, Stuttgart Univ., NASA TM 88534, 1983.

[4]van Dam, C. P., "Induced-Drag Characteristics of Crescent-Moon-Shaped Wings," *Journal of Aircraft*, Vol. 24, No. 2, 1987, pp. 115–119.

[5]Maskew, B., "Prediction of Subsonic Aerodynamics Characteristics: A Case for Low-Order Panel Methods," *Journal of Aircraft*, Vol. 19, No. 2, 1982, pp. 157–163.

[6]Vijgen, P. M. H. W., van Dam, C. P., and Holmes, B. J., "Sheared Wing-Tip Aerodynamics: Wind Tunnel and Computational Investigation," *Journal of Aircraft*, Vol. 26, No. 3, 1989, pp. 207–213.

[7]Gosse, A. J., British Aerospace Plc Memorandum, FD/SPARV/53, 1987.

[8]Petrie, J. A. H., "Development of an Efficient and Versatile Panel Method for Aerodynamic Problems," Ph.D. Dissertation, Leeds Univ., Leeds, England, UK, 1979.

[9]van Dam, C. P., Vijgen, P. M. H. W., and Holmes, B. J., "Wind-Tunnel Investigation on the Effect of the Crescent Planform Shape on Drag," AIAA Paper 90-0300, Jan. 1990.

[10]Naik, D. A., "An Investigation of the Aerodynamic Characteristics of Planar and Nonplanar Outboard Wing Planforms," Ph.D. Dissertation, Texas A&M Univ., College Station, TX, 1987.

[11]DeHaan, M. A., "Induced Drag of Wings with Highly Swept and Tapered Wing Tips," AIAA Paper 90-3062-CP, Jan. 1990.

[12]Fage, A., "The Effect of Narrow Spanwise Surface Ridge on the Drag of a Laminar Flow Aerofoil," Aeronautical Research Council, R&M 2120, London, 1943.

[13]Glauert, H., *The Elements of Aerofoil and Airscrew Theory*, Cambridge Univ. Press, 1926, Chaps. X and XI, pp. 125–155.

[14]Chu, J. K., Rios-Chiquete, P., Sarohia, S., and Bernstein, L., "The Chu Tube: A Velocimeter for Use in Highly-Sheared, Three Dimensional Steady Flows," *Aeronautical Journal of Royal Aeronautical Society*, March 1987, pp. 142–149.

[15]Lam, F., "Induced Drag and Wake Structures Behind Wings," Ph.D. Dissertation, Cambridge Univ., 1991.

[16]Goldstein, S., *Modern Developments in Fluid Dynamics*, Dover, London, 1965, pp. 257–259.

[17]Maskell, E. C., "Progress Towards a Method for the Measurement of the Components of the Drag of a Wing of Finite Span," Royal Aerospace Establishment, TR 72232, Cambridge, England, UK, 1972.

[18]Yates, J. E., and Donaldson, C., du P., "A Fundamental Study of Drag and an Assessment of Conventional Drag-Due-to-Lift Reduction Devices," NASA CR 4004, June 1986.

[19]Hamidy, E., "A Study of Road Vehicle Wakes," M.S. Thesis, Imperial College, London, 1985.

[20]Brune, G. W., and Bogataj, P. W., "Induced Drag of a Simple Wing from Wake Measurements," 1990 SAE Aerospace Technology Conf. and Exposition, Oct. 1990.

[21]Batchelor, G. K., "Axial Flow in Trailing Line Vortices," *Journal of Fluid Mechanics*, Vol. 20, Pt. 4, 1964, pp. 645–658.

[22]Batchelor, G. K., *An Introduction to Fluid Dynamics*, Cambridge Univ. Press, 1970, Chap. III, pp. 156–164.

[23]Clements, R. R., and Maull, D. J., "The Rolling up of a Trailing Vortex Sheet," *Aeronautical Journal of Royal Aeronautical Society*, Britain, Jan. 1973, pp. 46–51.

[24]van Dam, C. P., Vijgen, P. M. H. W., and Holmes, B. J., "High-α Characteristics of Crescent and Elliptic Wings," AIAA Paper 89-2240, July 1989.